2D Materials

OPEN ACCESS

RECEIVED
21 June 2025

REVISED
22 August 2025

ACCEPTED FOR PUBLICATION
2 September 2025

PUBLISHED
12 September 2025

PAPER

Clean transfer of two-dimensional materials using UV-ozone treated polydimethylsiloxane

Han Yan[1], Kamal Kumar Paul[1], Lixin Liu[1], Hao Wang[2], Huiyu Huang[2], Deepnarayan Biswas[3], Tien-Lin Lee[3], Manish Chhowalla[1,*] and Yan Wang[1,*]

[1] Department of Materials Science & Metallurgy, University of Cambridge, 27 Charles Babbage Road, Cambridge CB3 0FS, United Kingdom
[2] Department of Engineering, University of Cambridge, 9 JJ Thomson Ave, Cambridge CB3 0FA, United Kingdom
[3] Diamond Light Source, Harwell Science and Innovation Campus, Didcot OX11 0DE, United Kingdom
[*] Authors to whom any correspondence should be addressed.

E-mail: mc209@cam.ac.uk and yw472@cam.ac.uk

Keywords: 2D materials, clean transfer, field-effect transistors, solar cells, transition metal dichalcogenides

Supplementary material for this article is available online

Abstract

The clean and reliable transfer of two-dimensional (2D) materials is critical for preserving their intrinsic properties and enabling high-performance device applications. This study presents a method utilising UV-ozone treated polydimethylsiloxane (UV-PDMS) as a transfer medium to achieve residue-free 2D materials. The UV-PDMS transfer method increases surface rigidity, reduces surface polymeric residues, and ensures intimate contact between 2D materials and target substrates. This is translated into cleaner samples as confirmed by atomic force microscopy, photoluminescence spectroscopy, and x-ray photoelectron spectroscopy. Field-effect transistors based on monolayer MoS_2 fabricated with UV-PDMS transferred method exhibit lower subthreshold swing, reduced hysteresis, and higher carrier mobility compared to devices fabricated with PDMS transfer. Additionally, vertical solar cells based on multilayer WSe_2 prepared with UV-PDMS method demonstrate enhanced fill factor and power conversion efficiency.

The semiconducting properties of two-dimensional (2D) materials, such as transition metal dichalcogenides (TMDs), have sparked significant interest for their use in electronic and optoelectronic applications [1–3]. These materials exhibit remarkable electrical, optical, and mechanical properties that make them attractive for a variety of device applications, including field-effect transistors (FETs), photovoltaics, memories, and sensors [4–6]. To enable scalable fabrication process, large-area synthesis techniques such as metal organic and thermal chemical vapour deposition (CVD) have been developed for the growth of 2D TMDs [7, 8]. However, the growth of TMDs typically requires high temperature that exceed the thermal budget of back-end-of-line fabrication constraints [9]. Furthermore, strong interfacial coupling between CVD-grown 2D TMD films and their underlying substrates often leads to degraded carrier mobility, thereby limiting the performance of devices on as-grown substrates [10]. To overcome these issues, effort has been put into developing clean transfer of 2D TMDs onto target substrates for further device fabrication and tests [11–23].

A suitable transfer medium is crucial for transferring atomically thin and delicate 2D TMDs onto target substrates [11]. Although various polymer-based transfer media, including polymethyl methacrylate (PMMA), polystyrene, polycarbonate (PC), and polyvinyl alcohol (PVA), have been commonly employed, these materials typically introduce insulating residues and mechanical damage during delamination or cleaning [11–14]. Moreover, these processes require dissolving polymers with organic solvents such as chloroform, which can introduce unintentional doping in 2D materials [15]. The key challenge lies in developing a clean and reliable transfer method that preserves intrinsic properties of 2D materials [16–18]. Recent advances utilising silicon

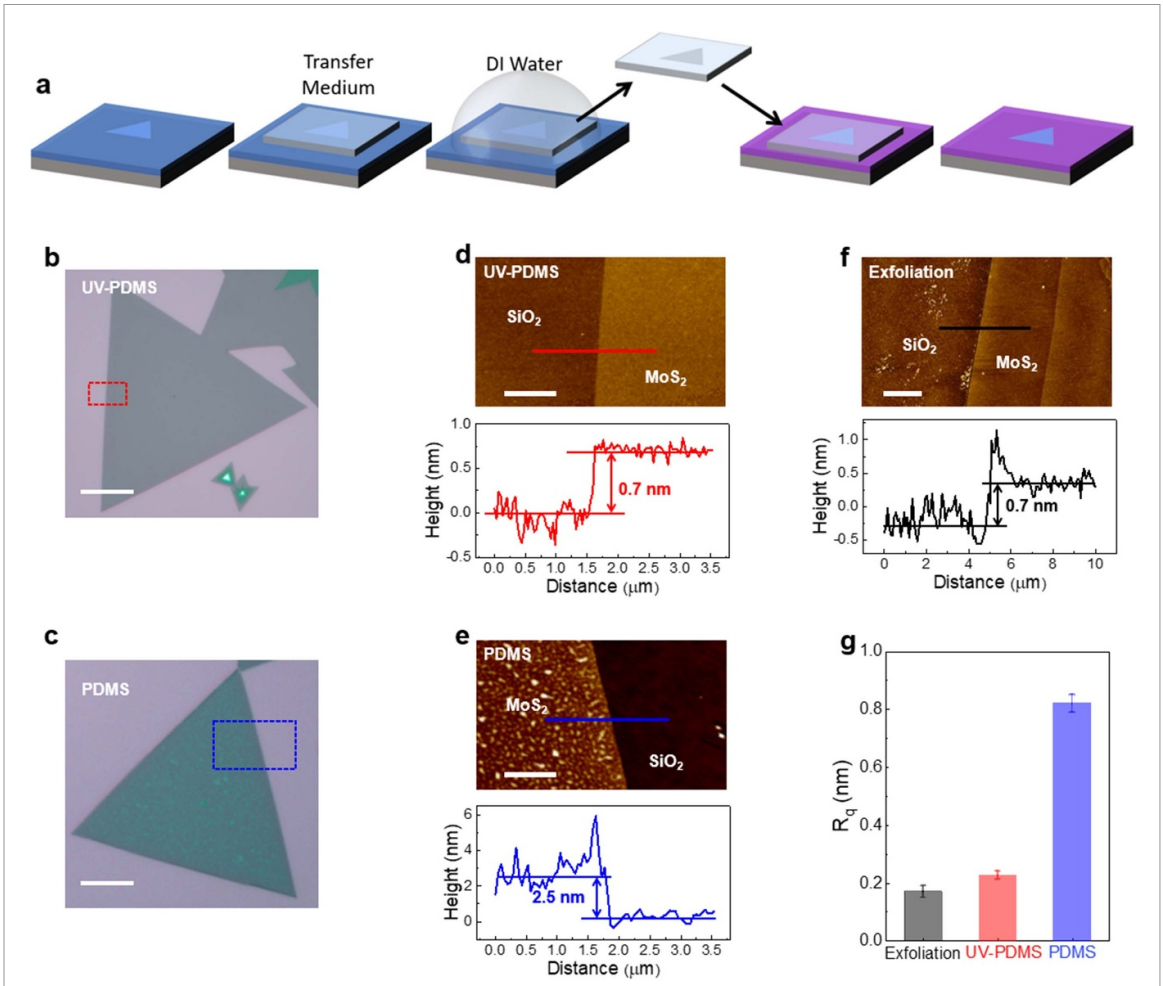

Figure 1. (a), Schematic of surface-energy-assisted transfer process using a transfer medium (PDMS or UV-PDMS). A CVD-grown MoS_2 flake on a SiO_2/Si growth substrate is first brought into contact with a transfer medium. DI water is introduced at the interface, enabling the MoS_2 flake to detach and adhere to the transfer medium. This assembly is then aligned and brought into contact with the target substrate. Finally, the transfer medium is removed, leaving the MoS_2 flake on the target surface. (b), (c), Optical microscope images of MoS_2 transferred onto SiO_2/Si substrates using UV-PDMS (b) and PDMS (c), respectively. Scale bars: 10 μm (b) and 7.5 μm (c). (d)–(f), AFM image and profile of (d) UV-PDMS transferred CVD-grown monolayer MoS_2 on SiO_2, (e) PDMS transferred CVD-grown monolayer MoS_2 on SiO_2, (f) Blue tape exfoliated monolayer MoS_2 on SiO_2. Scale bars: 2 μm. (g), Root mean square roughness of MoS_2 on SiO_2 substrates prepared via different preparation methods, indicating UV-PDMS method yields similar surface quality to those obtained by direct exfoliation. Data are extracted from AFM analysis.

nitride membranes, PMMA modified with oxhydryl group, ice-assisted transfer, and low-residue polypropylene carbonate have shown considerable improvements in maintaining surface cleanliness and improving device performance [16, 17, 19, 20]. By reviewing and evaluating these transfer approaches, three critical principles emerge for achieving clean transfers [16–18, 21–23]. First, choosing transfer media that leave minimal residue—non-polymeric materials preferred. Second, ensuring that the surface of the transfer medium is sufficiently rigid to prevent formation of bubble or blister. Finally, minimising the use of additional chemical cleaning steps to reduce the risk of introducing further perturbations.

In this study, we adopted a transfer approach utilising UV-ozone treated polydimethylsiloxane (abbreviated as UV-PDMS hereafter), where the PDMS can either be fabricated in-house or commercially available PF X4 gel film from Gel-Pak [24]. The UV-ozone PDMS method was reported by Jain *et al* for transferred mechanical exfoliated MoS_2, showing much reduced residue [24]. In this study, we have extended this method to clean transfer of CVD grown monolayer MoS_2. The cleanliness of the UV-PDMS transferred 2D materials were systematically evaluated through atomic force microscopy (AFM), photoluminescence (PL) spectroscopy, and x-ray photoelectron spectroscopy (XPS). Furthermore, FETs and photovoltaic devices based on 2D materials fabricated using UV-PDMS as transfer medium exhibited improved performance compared to those using untreated PDMS, highlighting the importance of minimising contaminations and enhancing interface integrity.

Detailed transfer process of CVD MoS_2 is illustrated in figure 1(a). Initially, MoS_2 flakes synthesised via CVD on SiO_2 substrates were contacted directly with a piece of transfer medium (PDMS

or UV-PDMS). Subsequently, deionized (DI) water was introduced around the perimeter of the transfer medium, allowing water to intercalate between the hydrophobic MoS_2 flakes and the hydrophilic SiO_2 surface [19, 25, 26]. As a result, when the transfer medium was gently lifted at a speed of approximately 50 μm s^{-1} at room temperature, the MoS_2 flakes detached from the growth substrate and adhered securely to the transfer medium, driven by surface energy interactions. The transfer medium carrying the MoS_2 flakes was then dried by blowing argon gas and heating on a hot plate at 80 °C for 20 min. Afterwards, the transfer medium was brought into contact with the target substrate, and the MoS_2 flakes were effectively transferred by gently removing the transfer medium at a temperature below 80 °C, with a lifting speed of approximately 5 μm s^{-1}. These conditions align with studies emphasising the influence of lifting speed and temperature on the transfer of 2D materials [27, 28]. This approach preserves the integrity of MoS_2 flakes without the need for aggressive acid or alkali etching that is typically required for PMMA assisted transfer. The cleanliness of the transfer method was initially assessed by comparing optical microscope images of MoS_2 flakes transferred onto new SiO_2/Si substrates using untreated PDMS and UV-PDMS, shown in figures 1(b) and (c). The images clearly demonstrate that UV-PDMS provides better transfer quality, characterised by fewer visible residues and improved surface uniformity compared to PDMS transfer. In addition to this improvement, it is worth noting that UV-PDMS transfer achieves a residue-free interface while retaining the mechanical simplicity, flexibility, and scalability of polymer-based methods. Unlike recent solvent-free clean transfer techniques, which require specialised materials and procedures [17, 29, 30], UV-PDMS enables robust, large-area transfer using readily available materials and equipment.

AFM results further quantify the morphology of monolayer MoS_2 transferred onto new SiO_2 substrates using UV-PDMS (figure 1(d)), and PDMS (figure 1(e)). In addition, mechanically exfoliated monolayer MoS_2 obtained by blue tape method, widely recognised for producing the cleanest 2D material samples, were characterised as a benchmark (figure 1(f)) [31, 32]. The main limitation of the blue tape method is that it yields only a limited number of flakes suitable for device fabrication. The directly exfoliated sample exhibits a thickness of less than 1 nm, consistent with the theoretical monolayer thickness of MoS_2 [33]. UV-PDMS transferred CVD monolayer MoS_2 show comparable thicknesses with minimal residue, whereas PDMS transferred samples show thicknesses exceeding 2 nm along with significantly rougher surface morphologies, indicative of polymer residues and trapped blisters. The root mean square roughness analysis of monolayer MoS_2 prepared by PDMS transfer, UV-PDMS transfer, and direct exfoliation are summarised in figure 1(g). The results show UV-PDMS transferred samples exhibit significantly improved cleanliness, approaching the quality of directly exfoliated monolayers. The non-idea characteristics in PDMS transferred samples primarily arises from polymeric surface and intrinsic softness of untreated PDMS.

The enhanced surface cleanliness achieved using UV-PDMS has significant impact for subsequent device fabrication processes, as shown in figure S1. The PDMS transferred MoS_2/SiO_2 sample exhibits poor wettability, leading to non-uniform spin-coating of electron beam resist (methyl methacrylate, MMA). Conversely, UV-PDMS method effectively minimises surface residues, producing a hydrophilic surface that facilitates uniform MMA coating [27]. A uniform resist coating improves feature resolution and prevents defects that could arise from inconsistent resist adhesion, thereby enhancing the reproducibility and performance of devices based on 2D materials.

To further characterise the chemical nature and origin of residues associated with different transfer methods, x-ray photoemission emission spectroscopy was performed on PDMS and UV-PDMS. Figure 2(a) presents the Si 2*p* core-level spectrum of untreated PDMS, revealing a dominant contribution from Si–C bonds compared to Si–O bonds. This spectral dominance originates from the intrinsic chemical structure of PDMS, as shown schematically in the inset, where silicon atoms are predominantly bonded to carbon-containing methyl side groups. Upon UV-ozone treatment, the Si 2*p* spectrum of UV-PDMS (figure 2(b)) exhibits an evident shift in spectral dominance from Si–C to Si–O species. This shift is a direct consequence of the oxidation process, where methyl side groups in PDMS are replaced by silanol groups through exposure and cross-linking of Si–O chains. The resulting surface becomes more rigid and silica-like, with a significant reduction in surface oligomers, as illustrated in the inset schematic. The mechanical effect of this surface modification is also evident in figure S2, with untreated PDMS readily deforms under the pressure of a tweezer tip and UV-treated PDMS exhibits a markedly stiffer response. In addition, the XPS survey spectra also shows a higher O 1*s* to Si 2*s* intensity ratio in UV-PDMS compared to PDMS samples, consistent with increased surface oxidation.

Following the confirmation of surface oxidation on UV-PDMS, its effectiveness in minimising residue post 2D material transfer was evaluated by high resolution synchrotron XPS, measuring single flake samples on target substrates (SiO_2 in figure 2(c) and ZrO_2 in figure 2(d)). As shown in figure 2(c), the

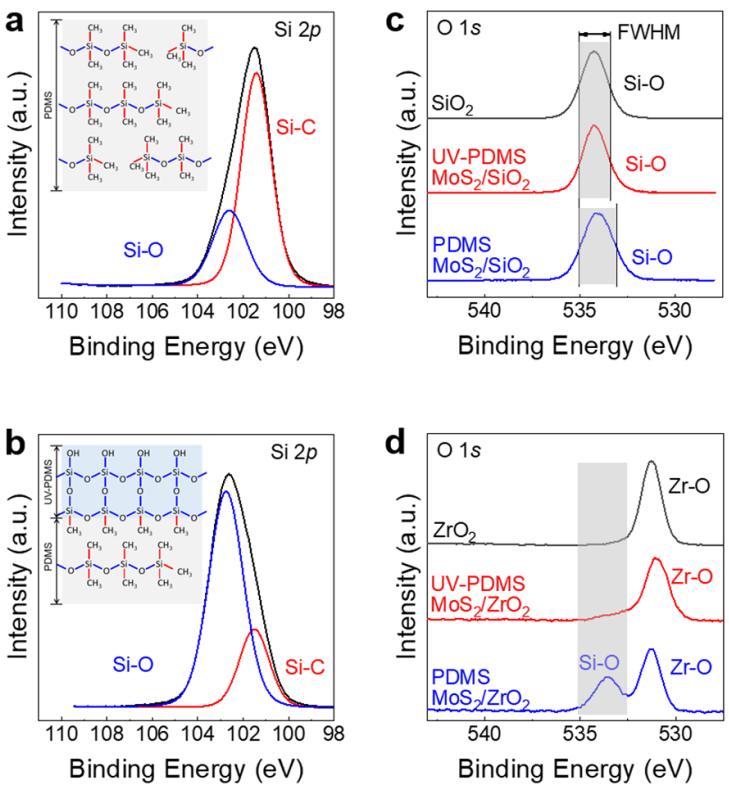

Figure 2. (a), Si 2*p* core-level spectrum of PDMS, showing a dominant contribution from Si–C species compared to Si–O. Inset: schematic of PDMS chemical structure, highlighting the origin of Si–C and Si–O signals. (b), Si 2*p* c core-level spectrum of UV-PDMS, exhibiting a dominant Si–O contribution over Si–C after UV-ozone treatment. Inset: schematic of UV-PDMS chemical structure, illustrating the mechanism behind the shift in spectral dominance. (c), O 1*s* core-level XPS spectra of a SiO_2 substrate, SiO_2 covered with CVD-grown monolayer MoS_2 transferred via UV-PDMS, and SiO_2 covered with CVD-grown monolayer MoS_2 transferred via PDMS. The increased FWHM of the O 1*s* peak in PDMS-transferred sample suggests the presence of PDMS residue. (d), O 1*s* core-level XPS spectra of a ZrO_2 substrate, ZrO_2 covered with CVD-grown monolayer MoS_2 transferred via UV-PDMS, and CVD-grown monolayer ZrO_2 covered with MoS_2 transferred via PDMS. The additional Si–O species in the PDMS-transferred sample originates from PDMS residue.

O 1*s* spectrum of the pristine SiO_2 substrate exhibits a single, well-defined peak with full width at half maximum (FWHM) of 1.60eV. The O 1*s* of the UV-PDMS transferred MoS_2 on SiO_2 shows a similar characteristic of pristine SiO_2, indicating that UV-ozone treatment can effectively suppress PDMS residues. In contrast, the SiO_2 substrate with MoS_2 transferred using PDMS displays a broader O 1*s* peak, evidenced by an increased FWHM of 1.89 eV. This is attributed to additional signals from Si–O species originating from PDMS residues that left on the sample surface after transfer. A more distinct comparison is provided by the O 1*s* spectra of CVD-grown monolayer MoS_2 transferred onto ZrO_2 substrates, as presented in figure 2(d). The O 1*s* spectrum of the pristine ZrO_2 substrate exhibits a single, well-defined peak. In the UV-PDMS transferred sample, this clean spectral profile is preserved. In contrast, the PDMS-transferred sample shows an additional peak corresponding to Si–O species, clearly indicating the presence of PDMS residue on transferred MoS_2.

Monolayer MoS_2 transferred by different methods were further assessed by PL and Raman spectroscopies, as summarised in figure 3. Figure 3(a) presents the PL spectra of monolayer MoS_2 on SiO_2 substrates, prepared by mechanical exfoliation, UV-PDMS transfer, and PDMS transfer methods. The UV-PDMS transferred sample exhibits a PL line shape nearly identical to that of the mechanically exfoliated benchmark, featuring lower intensities and a trion-dominant peak (trion denoted as A–) due to SiO_2 doping [34–36]. In contrast, the PDMS-transferred sample shows a more intense, exciton-dominated spectrum (exciton denoted as A), suggesting that trapped bubbles and PDMS residues can substantially influence interactions between MoS_2 and dielectrics, altering the surface charge transfer induced doping of MoS_2. PL deconvolution results are shown in figure S3. Figure 3(b) shows a quantitative comparison of the exciton proportion, defined as $I_A/(I_A + I_{A-})$, where I_A and I_{A-} stand for exciton intensity and trion intensity, respectively. The PDMS transferred samples show an average exciton proportion of around 0.6, while the exfoliated and UV-PDMS transferred samples show significantly lower values, typically below 0.1. The smaller error bars associated with the UV-PDMS and mechanically exfoliated samples reflect more uniform spectral characteristics, whereas the PDMS transferred samples demonstrate greater variability, indicative of less consistent optical quality

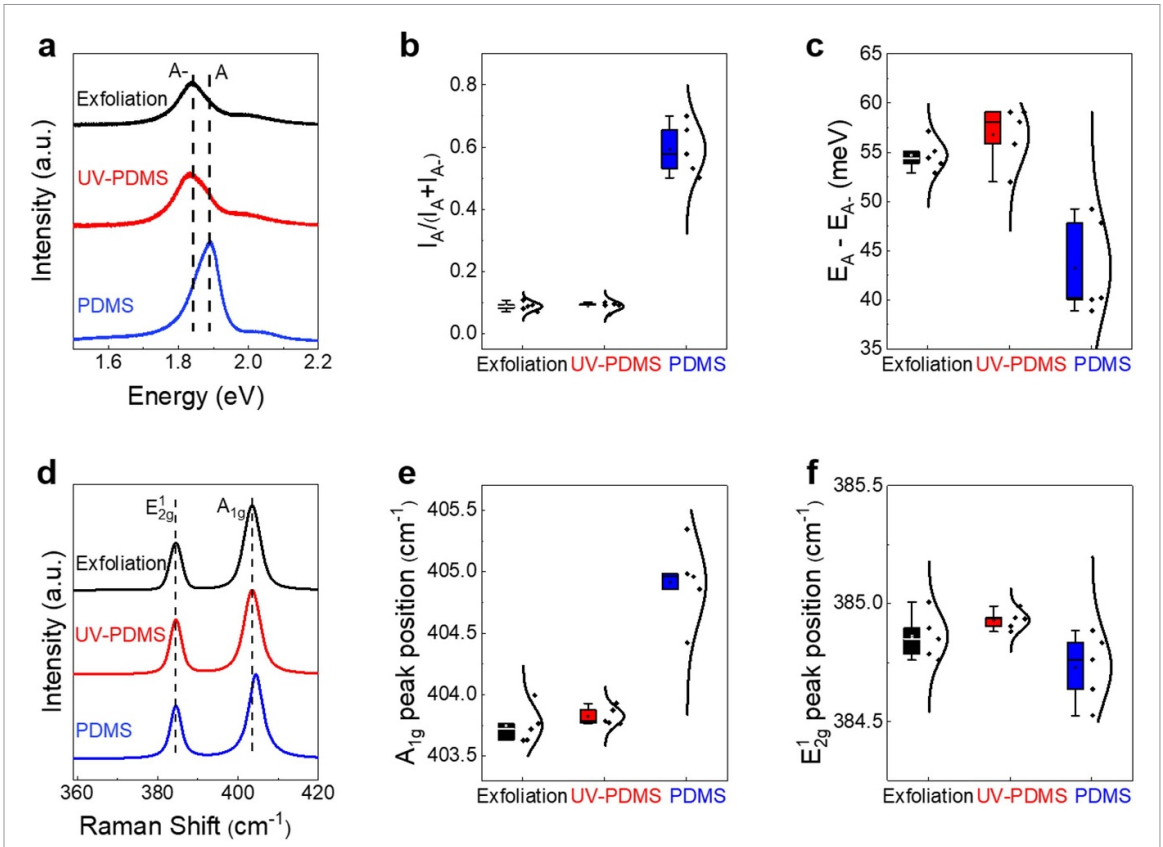

Figure 3. (a), PL spectra of monolayer MoS_2 on SiO_2 substrates prepared by exfoliation, UV-PDMS transfer, and PDMS transfer methods. (b), Comparison of exciton proportions of monolayer MoS_2 prepared via different transfer methods. (c), Comparison of energy differences between exciton and trion peaks of monolayer MoS_2 prepared via different fabrication methods. (d), Raman spectra of monolayer MoS_2 on SiO_2 substrates prepared by exfoliation, UV-PDMS transfer, and PDMS transfer methods. (e), Comparison of A_{1g} peak positions of monolayer MoS_2 prepared via different fabrication methods. (f), Comparison of E^1_{2g} peak positions of monolayer MoS_2 prepared via different fabrication methods.

across the samples. Additionally, figure 3(c) presents the energy separation between the exciton and trion peaks—commonly referred to as the trion binding energy-which is influenced by the degree of dielectric screening experienced by MoS_2 [34, 37, 38]. The reduced trion binding energies observed in PDMS transferred samples suggest the formation of a non-contact interface, which may degrade device performance by weakening electrostatic gate control.

Raman spectroscopy was also used to examine strain and doping effects in the MoS_2/SiO_2 samples. It is well established that E^1_{2g} mode is sensitive to strain in MoS_2, whereas A_{1g} mode is more responsive to changes in electron concentration [39]. Comparisons of the extracted A_{1g} peak positions (figure 3(e)) reveal a blueshift in PDMS transferred samples compared to mechanically exfoliated and UV-PDMS transferred samples. This suggests a lower electron concentration in PDMS transferred MoS_2, resulting from weaker substrate-induced doping due to poor interfacial contact with SiO_2 substrate. The E^1_{2g} peak positions (figure 3(f)) remain largely consistent across all samples, indicating that strain levels are comparable. Therefore, the spectral variations are predominantly governed by differences in sample cleanliness.

To demonstrate the versatility of the UV-PDMS transfer process, CVD-grown MoS_2 was successfully transferred onto photoresin substrates patterned with holes, forming suspended structures (figure S4(a)). This suspended configuration is known to enhance optoelectronic performance and strain tunability, making it attractive for photonic and nanoelectromechanical applications [40, 41]. As shown in figure S4(b), the PL spectrum of suspended MoS_2 exhibits significantly increased intensity compared to that of MoS_2 on photoresin, known to be a characteristic feature of clean suspended monolayer MoS_2 [42, 43].

Bottom-gated FETs were fabricated using CVD-grown monolayer MoS_2 transferred onto ZrO_2 by UV-PDMS and PDMS methods. The fabrication process followed the procedures described in the Methods section. Figures 4(a) and (b) show the device schematic and measurement configuration. The transfer characteristics of FETs based on monolayer MoS_2 transferred using PDMS and UV-PDMS are shown in figure 4(c). The devices fabricated with UV-PDMS transferred MoS_2 exhibited lower subthreshold swing (SS), reduced hysteresis, and higher ON-state current compared to those transferred with PDMS. Figure 4(d) shows the output

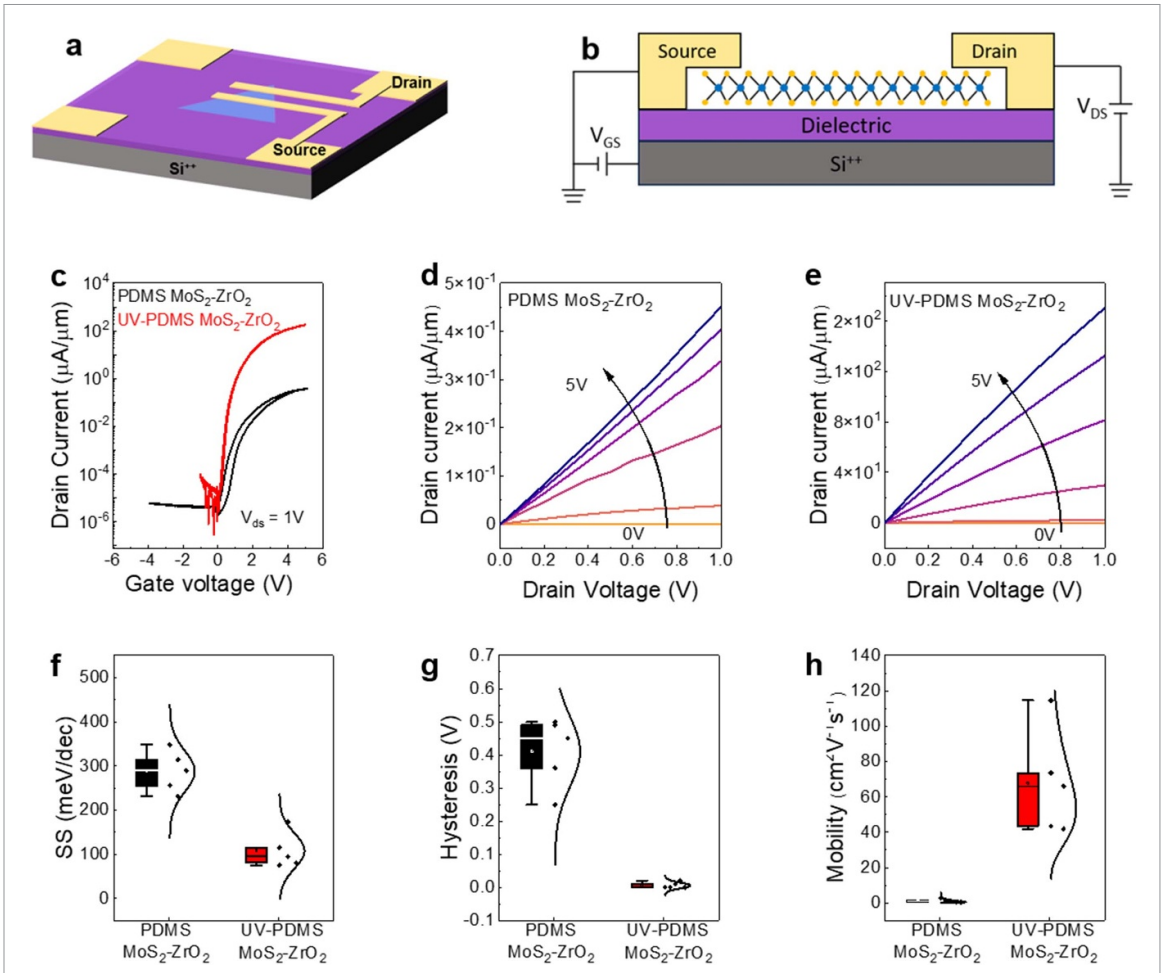

Figure 4. (a), (b), Schematics of three-terminal FET based on monolayer MoS_2 with heavily doped silicon (Si^{++}) bottom gate. (c), Logarithmic transfer curves of FETs based on CVD-grown monolayer MoS_2 transferred onto ZrO_2 using PDMS and UV-PDMS. (d), Output characteristics of a FET fabricated with PDMS transferred CVD-grown monolayer MoS_2 on ZrO_2. (e), Output characteristics of a FET with UV-PDMS transferred CVD-grown monolayer MoS_2 on ZrO_2. (f)–(h), Statistical distribution of (f) SS, (g) hysteresis, (h) mobility for FETs fabricated from PDMS and UV-PDMS transferred CVD-grown monolayer MoS_2.

characteristics of a FET based on PDMS transferred MoS_2, which shows low current levels around 0.5 μA μm^{-1} due to low mobility, poor electrostatic doping, and high contact resistance [44]. In contrast, the output curves of FET based on UV-PDMS transferred MoS_2 show improved linearity and higher current level up to 200 μA μm^{-1} (figure 4(e)). To provide a more comprehensive comparison, statistical distributions of key performance parameters extracted from the transfer characteristics are shown in figures 4(f) and (g). Devices fabricated using UV-PDMS consistently exhibited lower SS values, averaging 107 $\pm$ 35 mV dec^{-1} with a minimum of 75 mV dec^{-1}, compared to 288 $\pm$ 41 mV dec^{-1} for those transferred with PDMS (figure 4(f)). This improvement indicates a higher-quality MoS_2/dielectric interface, leading to enhanced electrostatic gate control. Figure 4(g) highlights the negligible hysteresis voltage observed in UV-PDMS transferred devices, in contrast to 410 $\pm$ 90 mV in devices transferred using PDMS. This reduction is attributed to minimised interfacial contamination, resulting in fewer charge trapping sites. Additionally, FETs fabricated on UV-PDMS transferred samples exhibit one order of magnitude higher (67.9 $\pm$ 26.4 cm^2 V^{-1} s^{-1}, peaking at 114 cm^2 V^{-1} s^{-1}) mobilities compared to PDMS transferred samples (1.2 $\pm$ 0.8 $cm^2V^{-1}s^{-1}$). Using the Y-function method [45, 46], the contact resistance for UV-PDMS transferred devices is extracted as 3.71 $\pm$ 0.22 k$\Omega\cdot\mu$m, whereas for PDMS transferred devices it is significantly higher at 136.61 $\pm$ 36.19 k$\Omega\cdot\mu$m. These substantial improvements can be ascribed to better electrostatic control, reduced scattering, and lower contact resistance between MoS_2 and the source/drain electrodes due to the elimination of PDMS residues [16].

Sample cleanliness can also influence photovoltaic performance of the devices based on multilayer TMD materials. We fabricated Pt/WSe_2/Al vertical diodes using multilayer WSe_2 (>50 nm thick) with PDMS and UV-PDMS transfer methods, as shown

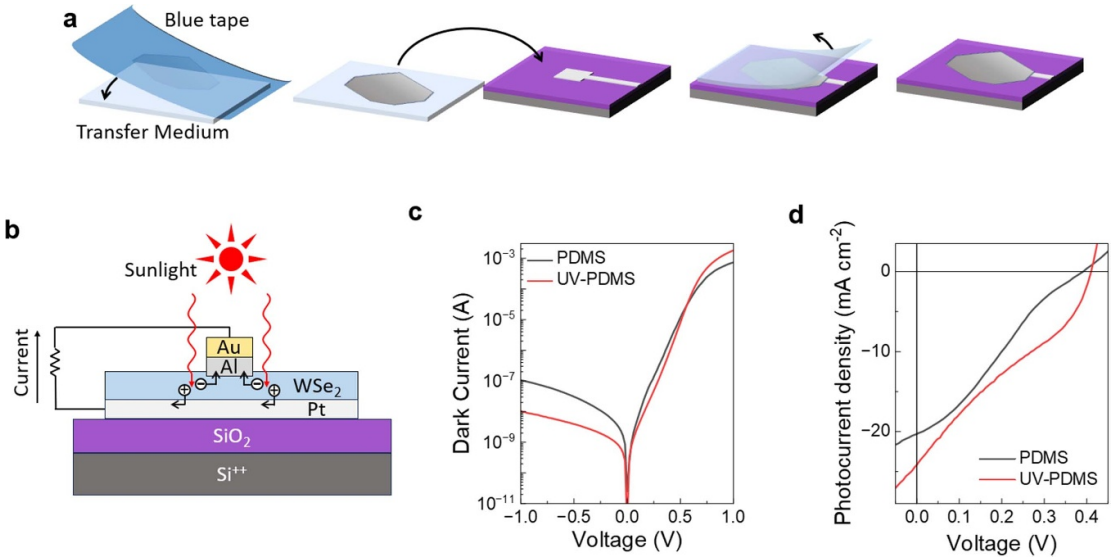

Figure 5. (a), Schematic showing the transfer process for making vertical photovoltaic devices using a transfer medium (PDMS or UV-PDMS). Multilayer WSe_2 flakes are first exfoliated directly onto the transfer medium. A selected flake is aligned and transferred onto a Pt bottom electrode on a SiO_2/Si substrate. The transfer medium is then slowly peeled away, leaving the WSe_2 flake precisely positioned on the target electrode. (b), Cross-sectional view of a vertical diode based on WSe_2 with Pt bottom contact and Al/Au top contact, showing its operation as a photovoltaic cell under 1-Sun illumination (AM 1.5 G). (c), Dark *I–V* curves of diodes fabricated using WSe_2 flakes transferred via PDMS and UV-PDMS. The device using UV-PDMS shows reduced leakage current under reverse bias, higher on/off ratio, and improved ideality factor. (d), *I–V* curves under 1-Sun illumination of diodes fabricated using WSe_2 flakes transferred via PDMS and UV-PDMS. The device using UV-PDMS shows improved photovoltaic performance.

schematically in figure 5(a). The WSe_2 flake is first exfoliated onto a transfer medium (PDMS or UV-PDMS) using blue tape and then aligned and stacked onto pre-patterned Pt electrodes on a SiO_2 substrate. Upon gentle removal of the transfer medium, the WSe_2 flake is successfully transferred on the Pt bottom electrode. Although the multilayer flakes are less susceptible to trapped bubbles due to their inherent rigidity, WSe_2 flake transferred with UV-PDMS exhibits minimal residue and significantly lower surface roughness (figure S5), demonstrating the effectiveness of UV-PDMS method in achieving cleaner multilayer TMD transfer.

The device configuration and measurement conditions are provided in figure 5(b). Upon illumination, electron-hole pairs are generated within the WSe_2 layer and separated by the built-in electric field established by the work function difference between the top and bottom electrodes. Figure 5(c) shows the dark current–voltage (*I–V*) characteristics of diodes fabricated using WSe_2 flakes transferred via PDMS and UV-treated PDMS. The device prepared with UV-PDMS shows one order of magnitude lower reverse leakage current and a steeper forward turn-on, corresponding to an on/off ratio of 1.7×10^5. In contrast, the device prepared with PDMS shows a much lower on/off ratio of 7.0×10^3. Diode quality is further assessed by the ideality factor, where a value of 1.0 corresponds to an ideal diode, as determined by fitting the Shockley diode equation to the dark *I–V* curves [47]. The device prepared using UV-PDMS gives an ideality factor of 1.78, whereas the device prepared using PDMS shows an ideality factor of 2.22. These differences reflect the better interfacial quality in the device prepared with UV-PDMS, which minimises charge trapping and facilitates near-ideal diode behaviour. Under 1-Sun illumination (AM 1.5 G), the device prepared using UV-PDMS demonstrates improved photovoltaic performance, as shown in figure 5(d). Specifically, the open-circuit voltage (V_{OC}) increases from 0.39 V (PDMS) to 0.41 V (UV-PDMS), and the short-circuit current density (J_{SC}) improves from 20.3 mA cm^{-2} to 24.1 mA cm^{-2}. Additionally, the fill factor rises from 25.9% to 27.5%, resulting in a power conversion efficiency (PCE) enhancement from 2.05% to 2.71%. These improvements highlight the crucial role of transfer-induced cleanliness in reducing interfacial recombination, improving contact quality, and enhancing overall photovoltaic device performance.

In conclusion, we have demonstrated that UV-ozone treated PDMS enables clean, residue-free transfer of 2D materials, significantly improving sample cleanliness compared to untreated PDMS. Systematic characterisations with AFM, Raman, and XPS confirm reduced surface residue and enhanced uniformity in transferred monolayer and multilayer TMDs. These improvements translate directly to better device performance, with FETs based on UV-PDMS transferred MoS_2 showing lower SS, reduced hysteresis, and higher mobility. UV-PDMS transferred WSe_2 also enhances the photovoltaic response of diodes, yielding lower leakage currents, improved diode ideality, and increase in PCE. These results

highlight UV-PDMS transfer is a versatile and scalable method for high-performance devices based on 2D materials.

1. Methods

UV-ozone treatment of PDMS: UV-PDMS was either fabricated in-house with a thickness of approximately 2 mm or prepared from Gel-Pak PF X4 gel film (17 mil thickness). PDMS was treated for approximately 30 min in a commercial UV-Ozone Cleaner (Ossila, 15 mW·cm^{-2} at 185 nm) and subsequently stored under ambient conditions for several hours prior to use. The UV-ozone treatment oxidised the PDMS surface, creating a silica-like (SiO_x), rigid, and hydrophilic structure. Exposure to air stabilised the surface hydrophilicity, providing optimal conditions for subsequent surface-energy-assisted transfer processes [24]. The treatment duration influences the thickness and rigidity of the silica-like layer and can be adjusted as needed; in this study, durations between 20 and 60 min produced comparable surface conditions and high transfer quality, while longer durations were not examined.

CVD MoS_2 synthesis: Monolayer MoS_2 was obtained by CVD growth using MoO_3 and sulphur as precursors. 5 mg MoO_3 powder was evenly distributed in an alumina boat and located at the centre of a single-zone tube furnace. SiO_2 substrates, spin-coated with 0.5 mg ml^{-1} NaOH promoter, were placed face-down on the MoO_3 boat. 60 mg sulphur powder in another alumina boat was located 17 cm upper stream at the edge of the furnace. Before starting growth, the tube was purged with 460 sccm N_2 for 15 min at 150 °C. The N_2 flow rate was then decreased to 60 sccm. The MoO_3 source was heated to 720 °C and kept for 10 min, while the temperature of sulphur stabilised at around 230 °C. After the growth is done, the sulphur source was pulled out of the heating zone, and the tube was cooled down in 460 sccm N_2 gas.

Device fabrication: Electron beam lithography was used to define source and drain electrodes for FETs based on CVD-grown monolayer MoS_2, as well as the top electrode for photovoltaic devices based on multilayer WSe_2. A two-layer e-beam resist, consisting of methyl methacrylate (MMA) EL6 at the bottom and 495 polymethyl methacrylate (PMMA) A6 on top, was employed. Metal electrode deposition was performed using electron beam evaporation under a base pressure of $\sim 1 \times 10^{-7}$ Torr. Indium-gold deposition was used for source and drain electrodes of FETs [44].

Sample characterisation: AFM data were obtained by Dimension Icon (Bruker) with peak-force tapping (ScanAsyst) mode. PL and Raman data was collected using a 514 nm laser excitation focused through a ×100 objective lens. The spectra were taken at an incident laser power of 50 μW, which was sufficiently low to avoid any damage to the sample. Lab-based XPS spectra were obtained using a Thermo Scientific Nexsa G2 XPS. Synchrotron XPS were collected at Beamline I09 at Diamond Light Source (UK), with a beam energy of 3 keV and an incidence angle of 40°. Electrical measurements of FETs were performed at room temperature in a Lakeshore vacuum probe station using a 4200-SCS Keithley. Dark current–voltage (I–V) characteristics of the photovoltaic devices were measured in a two-probe measurement system in an ambient atmosphere with a 4200-SCS Keithley. To determine the PCE of the photovoltaic devices under AM 1.5 G, I–V measurements were performed using a solar simulator (Oriel Sol3A, Newport) connected to a Keithley 2440 source meter. The lamp intensity was calibrated with a Si reference cell (Newport, Oriel 91 150 V) precisely placed at the sample position. I–V curves were recorded in a normal lab environment (temperature: 22 °C; humidity: 35%). $I-V$ characteristics were performed with a scan rate of 200 mV s^{-1} and a dwell time of 30 ms.

Data availability statement

All data that support the findings of this study are included within the article (and any supplementary files).

Acknowledgment

M C and Y W received funding from the European Research Council (ERC) Advanced Grant under the European Union's Horizon 2020 research and innovation programme (Grant Agreement GA 101019828-2D- LOTTO), EPSRC (EP/T026200/1, EP/T001038/1, EP/Z535680/1), Department of Science, Innovation and Technology and the Royal Academy of Engineering under the Chair in Emerging Technologies programme. M C and K K P acknowledge funding from Horizon Europe UK Research and Innovation (UKRI) Underwrite MSCA (EP/Y028287/1). We acknowledge Diamond Light Source for time on beamline I09 under Proposal SI30105, SI33391, and SI38086.

Author contributions

Han Yan 0009-0008-3376-1697
Data curation (lead), Formal analysis (lead), Writing – original draft (lead), Writing – review & editing (lead)

Kamal Kumar Paul
Data curation (supporting), Formal analysis (supporting), Writing – review & editing (supporting)

Lixin Liu
Visualization (supporting), Writing – review & editing (supporting)

Hao Wang
Data curation (supporting)

Huiyu Huang
Data curation (supporting)

Deepnarayan Biswas
Data curation (supporting)

Tien-Lin Lee
Data curation (supporting)

Manish Chhowalla
Funding acquisition (equal), Investigation (equal), Resources (equal), Supervision (equal)

Yan Wang 0000-0001-9241-3512
Funding acquisition (equal), Investigation (equal), Resources (equal), Supervision (equal)

References

[1] Lanza M and Radu I 2022 Electronic circuits made of 2D materials *Adv. Mater.* **34** 2207843
[2] Chhowalla M, Jena D and Zhang H 2016 Two-dimensional semiconductors for transistors *Nat. Rev. Mater.* **1** 1–15
[3] Wang Y, Sarkar S, Yan H and Chhowalla M 2024 Critical challenges in the development of electronics based on two-dimensional transition metal dichalcogenides *Nat. Electron.* **7** 638–45
[4] Fan D *et al* 2023 Two-dimensional semiconductor integrated circuits operating at gigahertz frequencies *Nat. Electron.* **6** 879–87
[5] Liu C, Guo J, Yu L, Li J, Zhang M, Li H, Shi Y and Dai D 2021 Silicon/2D-material photodetectors: from near-infrared to mid-infrared *Light Sci. Appl.* **10** 123
[6] Akinwande D, Petrone N and Hone J 2014 Two-dimensional flexible nanoelectronics *Nat. Commun.* **5** 5678
[7] Hoang A T, Qu K, Chen X and Ahn J H 2021 Large-area synthesis of transition metal dichalcogenides: via CVD and solution-based approaches and their device applications *Nanoscale* **13** 615–33
[8] Katiyar A K, Choi J and Ahn J H 2025 Recent advances in CMOS-compatible synthesis and integration of 2D materials *Nano Convergence* **12** 11
[9] You J, Hossain M D and Luo Z 2018 Synthesis of 2D transition metal dichalcogenides by chemical vapor deposition with controlled layer number and morphology *Nano Convergence* **5** 26
[10] Kurabayashi S and Nagashio K 2017 Transport properties of the top and bottom surfaces in monolayer MoS_2 grown by chemical vapor deposition *Nanoscale* **9** 13264–71
[11] Watson A J, Lu W, Guimaraes M H D and Stöhr M 2021 Transfer of large-scale two-dimensional semiconductors: challenges and developments *2D Mater.* **8** 032001
[12] Cheliotis I and Zergioti I 2024 A review on transfer methods of two-dimensional materials *2D Mater.* **11** 022004
[13] Pham P V, Mai T-H, Dash S P, Biju V, Chueh Y-L, Jariwala D and Tung V 2024 Transfer of 2D films: from imperfection to perfection *ACS Nano* **18** 14841–76
[14] Zhang S *et al* 2019 Wafer-scale transferred multilayer MoS_2 for high performance field effect transistors *Nanotechnology* **30** 174002
[15] Mao N, Chen Y, Liu D, Zhang J and Xie L 2013 Solvatochromic effect on the photoluminescence of MoS_2 monolayers *Small* **9** 1312–5
[16] Mondal A, Biswas C, Park S, Cha W, Kang S-H, Yoon M, Choi S H, Kim K K and Lee Y H 2023 Low Ohmic contact resistance and high on/off ratio in transition metal dichalcogenides field-effect transistors via residue-free transfer *Nat. Nanotechnol.* **19** 34–43
[17] Wang W *et al* 2023 Clean assembly of van der Waals heterostructures using silicon nitride membranes *Nat. Electron.* **6** 981–90
[18] Dong W, Dai Z, Liu L and Zhang Z 2023 Toward clean 2D materials and devices: recent progress in transfer and cleaning methods *Adv. Mater.* **36** 2303014
[19] Zhao Y *et al* 2022 Large-area transfer of two-dimensional materials free of cracks, contamination and wrinkles via controllable conformal contact *Nat. Commun.* **13** 4409
[20] Liu H *et al* 2023 Controlled adhesion of ice—Toward ultraclean 2D materials *Adv. Mater.* **35** 2210503
[21] Purdie D G, Pugno N M, Taniguchi T, Watanabe K, Ferrari A C and Lombardo A 2018 Cleaning interfaces in layered materials heterostructures *Nat. Commun.* **9** 5387
[22] Desai S B *et al* 2016 Gold-mediated exfoliation of ultralarge optoelectronically-perfect monolayers *Adv. Mater.* **28** 4053–8
[23] Hu Z *et al* 2023 Rapid and scalable transfer of large-area graphene wafers *Adv. Mater.* **35** 2300621
[24] Jain A, Bharadwaj P, Heeg S, Parzefall M, Taniguchi T, Watanabe K and Novotny L 2018 Minimizing residues and strain in 2D materials transferred from PDMS *Nanotechnology* **29** 265203
[25] Quellmalz A *et al* 2021 Large-area integration of two-dimensional materials and their heterostructures by wafer bonding *Nat. Commun.* **12** 917
[26] Gurarslan A, Yu Y, Su L, Yu Y, Suarez F, Yao S, Zhu Y, Ozturk M, Zhang Y and Cao L 2014 Surface-energy-assisted perfect transfer of centimeter-scale monolayer and few-layer MoS_2 films onto arbitrary substrates *ACS Nano* **8** 11522–8
[27] Onodera M, Wakafuji Y, Hashimoto T, Masubuchi S, Moriya R, Zhang Y, Watanabe K, Taniguchi T and Machida T 2022 All-dry flip-over stacking of van der Waals junctions of 2D materials using polyvinyl chloride *Sci. Rep.* **12** 21963
[28] Wakafuji Y, Onodera M, Masubuchi S, Moriya R, Zhang Y, Watanabe K, Taniguchi T and Machida T 2022 Evaluation of polyvinyl chloride adhesion to 2D crystal flakes *npj 2D Mater. Appl.* **6** 44
[29] Lee M *et al* 2025 Residue-free fabrication of 2D materials using van der Waals interactions *Adv. Mater.* **37** 2418669
[30] Wen S *et al* 2025 Contamination-free assembly of two-dimensional van der Waals heterostructures toward high-performance electronics and optoelectronics *Appl. Mater. Today* **43** 102657
[31] Novoselov K S, Jiang D, Schedin F, Booth T J, Khotkevich V V, Morozov S V and Geim A K 2005 Two-dimensional atomic crystals *Proc. Natl Acad. Sci.* **102** 10451–3
[32] Novoselov K S, Geim A K, Morozov S V, Jiang D, Zhang Y, Dubonos S V, Grigorieva I V and Firsov A A 2004 Electric field effect in atomically thin carbon films *Science* **306** 666–9
[33] Wieting T J and Verble J L 1971 Infrared and Raman studies of long-wavelength optical phonons in hexagonal MoS_2 *Phys. Rev. B* **3** 4286–92
[34] Mak K F, He K, Lee C, Lee G H, Hone J, Heinz T F and Shan J 2013 Tightly bound trions in monolayer MoS_2 *Nat. Mater.* **12** 207–11
[35] Scheuschner N, Ochedowski O, Kaulitz A-M, Gillen R, Schleberger M and Maultzsch J 2014 Photoluminescence of freestanding single- and few-layer MoS_2 *Phys. Rev. B* **89** 125406
[36] Sun Y, Wang R and Liu K 2017 Substrate induced changes in atomically thin 2-dimensional semiconductors: fundamentals, engineering, and applications *Appl. Phys. Rev.* **4** 011301
[37] Drüppel M, Deilmann T, Krüger P and Rohlfing M 2017 Diversity of trion states and substrate effects in the

optical properties of an MoS_2 monolayer *Nat. Commun.* **8** 2117
[38] Florian M, Hartmann M, Steinhoff A, Klein J, Holleitner A W, Finley J J, Wehling T O, Kaniber M and Gies C 2018 The dielectric impact of layer distances on exciton and trion binding energies in van der Waals heterostructures *Nano Lett.* **18** 2725–32
[39] Chakraborty B, Bera A, Muthu D V S, Bhowmick S, Waghmare U V and Sood A K 2012 Symmetry-dependent phonon renormalization in monolayer MoS_2 transistor *Phys. Rev. B* **85** 161403
[40] Manzeli S, Dumcenco D, Migliato Marega G and Kis A 2019 Self-sensing, tunable monolayer MoS_2 nanoelectromechanical resonators *Nat. Commun.* **10** 4831
[41] Li B *et al* 2015 Scalable transfer of suspended two-dimensional single crystals *Nano Lett.* **15** 5089–97
[42] Yu Y, Yu Y, Xu C, Cai Y-Q, Su L, Zhang Y, Zhang Y-W, Gundogdu K and Cao L 2016 Engineering substrate interactions for high luminescence efficiency of transition-metal dichalcogenide monolayers *Adv. Funct. Mater.* **26** 4733–9
[43] Chaste J *et al* 2018 Intrinsic properties of suspended MoS_2 on SiO_2/Si pillar arrays for nanomechanics and optics *ACS Nano* **12** 3235–42
[44] Wang Y, Kim J C, Wu R J, Martinez J, Song X, Yang J, Zhao F, Mkhoyan A, Jeong H Y and Chhowalla M 2019 Van der Waals contacts between three-dimensional metals and two-dimensional semiconductors *Nature* **568** 70–74
[45] Wang Y and Chhowalla M 2022 Making clean electrical contacts on 2D transition metal dichalcogenides *Nat. Rev. Phys.* **4** 101–12
[46] Chang H Y, Zhu W and Akinwande D 2014 On the mobility and contact resistance evaluation for transistors based on MoS_2 or two-dimensional semiconducting atomic crystals *Appl. Phys. Lett.* **104** 113504
[47] Wang H *et al* 2022 Approaching the external quantum efficiency limit in 2D photovoltaic devices *Adv. Mater.* **34** 2206122